Journal of Power Sources 245 (2014) 398–405

Contents lists available at SciVerse ScienceDirect

Journal of Power Sources

journal homepage: www.elsevier.com/locate/jpowsour

Electrochemical performance of solid oxide fuel cells having electrolytes made by suspension and solution precursor plasma spraying

M. Marr, J. Kuhn, C. Metcalfe, J. Harris, O. Kesler*

Department of Mechanical and Industrial Engineering, University of Toronto, 5 King's College Road, Toronto, ON M5S 3G8, Canada

HIGHLIGHTS

- SOFC electrolytes produced by plasma spraying from 3 suspensions and 1 solution.
- Evaluated for microstructure, permeability and electrochemical performance.
- Peak power density of 599 mW cm^{-2} and open circuit voltage of 1.00 V at 750 °C.
- First reported electrochemical data on SOFCs with SPPS electrolytes.

ARTICLE INFO

Article history:
Received 2 April 2013
Received in revised form
13 June 2013
Accepted 14 June 2013
Available online 27 June 2013

Keywords:
Solid oxide fuel cell (SOFC)
Electrolyte
Yttria-stabilized zirconia (YSZ)
Suspension plasma spray (SPS)
Solution precursor plasma spray (SPPS)

ABSTRACT

Yttria-stabilized zirconia (YSZ) electrolytes were deposited by suspension plasma spraying (SPS) and solution precursor plasma spraying (SPPS). The electrolytes were evaluated for permeability, microstructure, and electrochemical performance. With SPS, three different suspensions were tested to explore the influence of powder size distribution and liquid properties. Electrolytes made from suspensions of a powder with $d_{50} = 2.6$ μm were more gas-tight than those made from suspensions of a powder with $d_{50} = 0.6$ μm. A peak open circuit voltage of 1.00 V was measured at 750 °C with a cell with an electrolyte made from a suspension of $d_{50} = 2.6$ μm powder. The use of a flammable suspension liquid was beneficial for improving electrolyte conductivity when using lower energy plasmas, but the choice of liquid was less important when using higher energy plasmas. With SPPS, peak electrolyte conductivities were comparable to the peak conductivities of the SPS electrolytes. However, leak rates through the SPPS electrolytes were higher than those through the electrolytes made from suspensions of $d_{50} = 2.6$ μm powder. The electrochemical test data on SPPS electrolytes are the first reported in the literature.

1. Introduction

Metal-supported solid oxide fuel cells (SOFCs) are a promising technology for clean energy conversion. Cells with yttria-stabilized zirconia (YSZ) electrolytes produced by wet ceramic processing [1], vacuum plasma spraying [2], and atmospheric dry powder plasma spraying [3] have achieved open circuit voltages (OCVs) at or near the Nernst potential. Atmospheric plasma spraying with suspension- or solution-based feedstocks could potentially deposit thinner and more uniform electrolytes than those produced from a dry powder feedstock. Electrolytes have been produced by suspension plasma spraying (SPS) [4,5], though cell OCVs are not yet as high as those of cells with electrolytes produced by other methods. Solution precursor plasma spraying (SPPS) is worth investigating because it offers reduced process complexity and higher compositional flexibility compared to SPS. However, to date, electrochemical testing of cells with SPPS electrolytes has not been reported in the literature.

With SPS, the size distribution of the particles in the feedstock suspension affects the properties of the resulting coating. After the suspension is injected into the plasma, it breaks down into droplets which each contain multiple powder particles. As the liquid evaporates from the droplets, the particles will either agglomerate together or disperse as individual particles [6]. The smaller the particle, the more rapidly it is heated and accelerated by the plasma plume [7]. However, smaller particles also cool faster as the plasma loses energy, so depending on plasma power and stand-off distance, smaller particles can re-solidify prior to reaching the substrate. Furthermore, small particles have low momentum and are more easily deflected by the plasma plume as they approach the substrate, which causes them to impact at an angle with low

* Corresponding author. Tel.: +1 416 978 3835; fax: +1 416 978 7753.
E-mail address: kesler@mie.utoronto.ca (O. Kesler).

0378-7753/$ – see front matter © 2013 Elsevier B.V. All rights reserved.
http://dx.doi.org/10.1016/j.jpowsour.2013.06.092

normal velocity [8]. This impact behaviour increases coating roughness and forms regions of concentrated porosity.

The choice of suspension liquid is also important with SPS. In this article, some suspensions were made with mixtures of water, ethanol, and ethylene glycol. Relative to an equivalent volume of water, 70% and 33% less energy is needed to heat from room temperature and evaporate ethanol and ethylene glycol, respectively. Additionally, these liquids can add energy to the plasma through combustion. The enthalpies of combustion are approximately −22 and −20 kJ ml^{-1}, respectively, for ethanol and ethylene glycol. With typical suspension feed rates, the corresponding combustion enthalpy is small relative to the plasma enthalpy. However, combustion does not occur until multiple centimetres from the torch nozzle exit after the evaporated liquids have sufficiently mixed with air [9]. The combustion energy may partially offset the cooling of the plasma plume to help maintain the YSZ droplets in a molten state at substrate impact. Therefore, the use of flammable suspension liquids may permit the production of electrolytes using lower energy plasmas than would be needed with entirely water-based suspensions. Lowering the plasma energy reduces electrolyte segmentation cracking [10].

Other liquid properties, including viscosity and surface tension, are also important for their effect on the breakup behaviour of the suspension after injection. The viscosity of water and ethanol are similar, while the viscosity of ethylene glycol is more than 1 order of magnitude higher. The surface tensions of ethanol and ethylene glycol are approximately 70% and 35% lower, respectively, than that of water. Surface tension has a stronger influence than viscosity on the final droplet size distribution, and suspensions with lower surface tensions (higher We numbers) have wider size distributions [11]. Accordingly, the atomized droplets from water/ethanol/ethylene glycol-based suspensions likely have a wider size distribution than those from water-based suspensions. It may be more challenging to optimize the spray configuration for a wider droplet size distribution.

At this time, SPPS has not been extensively used to produce SOFC electrolytes. Jia and Gitzhofer [12] produced ceria-based electrolytes by induction plasma spraying of a solution feedstock in a vacuum, though coatings were relatively porous and no electrochemical test data were obtained. One variant on SPPS is a hybrid SPS/SPPS spray technique, which could be used to incorporate various additives into YSZ coatings to improve their conductivity or other properties. VanEvery et al. [13] plasma sprayed a suspension of yttria-partially-stabilized zirconia particles in a solution containing Yb and Nd precursors. These dopants were incorporated into the resulting coating and reduced its thermal conductivity, as was intended. Regarding SOFC electrolytes, co-doped ScYSZ has higher conductivity than YSZ [14], so Sc precursors could be added to a suspension of YSZ particles. Transition metal oxides such as Ni, Co, Fe, and Mn have been found to lower the sintering temperature of YSZ [15], so adding these elements to YSZ suspensions could increase the density of plasma sprayed electrolytes, though conductivity may be reduced. In the present study, however, SPPS was used alone to produce YSZ electrolytes without other additives.

With SPPS, the feedstock for YSZ coatings is a solution of dissolved salts of zirconium and yttrium. For the production of dense SPPS coatings, appropriate precursors must be selected. Muoto et al. [16] used zirconium acetate and yttrium nitrate as precursors to make dense yttria-partially-stabilized zirconia coatings. The thermal decomposition processes for these precursors are generally exothermic, which promotes complete reaction of the precursors to the target material (YSZ) and high droplet temperatures at impact. Additionally, the use of high concentration solutions improves coating density by encouraging solute precipitation throughout the volume of the droplet rather than just at the surface, which increases the size of the molten YSZ droplets at impact [17].

For this article, SOFC electrolytes were deposited by liquid-feed plasma spraying to compare four different feedstocks: three suspensions and one solution. The electrolytes were evaluated for permeability, microstructure, and electrochemical performance as part of full cells. For the electrolytes, the key electrochemical test results of interest were cell open circuit voltage (OCV) and series resistance (R_s).

2. Experimental procedure

2.1. Plasma spray processing

$Y_{0.15}Zr_{0.85}O_{1.925}$ electrolytes were produced from 4 different liquid-based feedstocks, which are described in Table 1. Suspensions 1 and 2 were made with powder from Inframat Advanced Materials (product no. 4039OR-8601, Manchester, CT), and suspension 3 was made with powder from Tosoh Corp. (product no. TZ-8YS, Tokyo, Japan). Suspension 1 was entirely water-based while suspensions 2 and 3 were made from a mixture of water, ethanol and ethylene glycol. The solution was made from zirconium acetate solution (product no. 413801, Sigma Aldrich Co., St. Louis, MO) and yttrium nitrate hexahydrate (product no. 12898, Alfa Aesar, Ward Hill, MA). These precursors were mixed in a ratio of 0.15 mol. Y to 0.85 mol. Zr.

The electrolytes were deposited using an Axial III DC plasma torch combined with a peristaltic pump-based liquid feed system (Northwest Mettech Corp., North Vancouver, BC, Canada). A schematic of the plasma spraying process is shown in Fig. 1. For each feedstock, electrolytes were deposited using 3 different plasma conditions, which were each used at 2 stand-off distances (Table 2). (Suspension 1 and the solution were not tested with the 102 kW plasma at 75 mm due to a limited number of substrates and anticipated lower deposition efficiencies. Therefore, 22 different feedstock/plasma condition/stand-off distance combinations were tested in total.)

The 160 kW plasma was used to achieve a high degree of particle melting at impact with all feedstocks. The 102 and 112 kW plasmas were tested to determine if the use of flammable suspension liquids, smaller powders, and/or solution-based feedstocks would enable the production of denser coatings using lower energy plasmas. The 102 kW condition used a smaller torch nozzle than the other conditions to produce a higher velocity plasma plume.

Table 1
Liquid feedstock characteristics.

Suspension details	Suspension 1	Suspension 2	Suspension 3	Solution
Powder d_{10} (μm)	0.8	0.8	0.2	Zirconium acetate + Yttrium nitrate
Powder d_{50} (μm)	2.6	2.6	0.6	Molar concentration = 2.2 mol l^{-1}
Powder d_{90} (μm)	5.7	5.7	1.5	
Powder vol.%	5	5	5	
H_2O vol.%	95	19	19	
Ethanol vol.%	0	38	38	
Ethylene glycol vol.%	0	38	38	

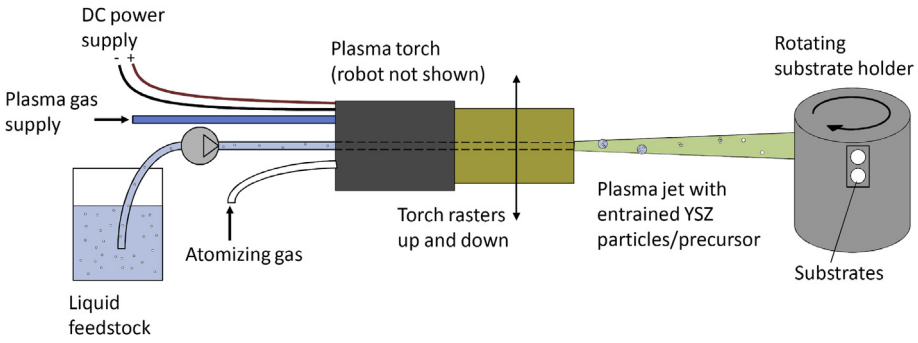

Fig. 1. Plasma spraying process schematic.

This smaller nozzle could not be used with higher plasma powers due to torch limitations. For each plasma condition, the two stand-off distances were chosen after preliminary trials to vary coating density and the degree of segmentation cracking. The suspensions were fed to the plasma at 14 ml min^{-1} and the solution was fed at 21 ml min^{-1}. With suspensions 2 and 3, this feed rate corresponds to a calculated combustion enthalpy addition of 3.5 kW. The feedstocks were injected into the plasma through a 0.84 mm inner diameter syringe tube, and the atomizing gas flow rate was 20 slpm. The target thickness for each electrolyte was 35 μm, though actual thicknesses varied because deposition efficiencies were not previously known for all deposition conditions and feedstocks.

The electrolytes were deposited on two types of substrates (Table 3). Each substrate had a diameter of 25.4 mm and a thickness of approximately 1.6 mm. The porous steel substrates were made of 430 stainless steel with a media grade (MG) 0.2 μm pore structure. The MG designation indicates the largest diameter of particles that should pass through the disks if they were being used as filters; it does not directly indicate pore size. The bi-layer anode substrates consisted of Ni–YSZ functional and bridging layers on 430 stainless steel supports with MG 1 μm pore structures. The functional layer was deposited by SPS as described in Ref. [18], and the bridging layer was deposited by plasma spraying a dry powder feedstock as described in Ref. [19].

During electrolyte deposition, the substrate holding fixture was mounted on a rotating turntable and the torch was mounted to a robot that rastered vertically. With this configuration, the torch passed in front of the substrate at 380 cm s^{-1}. At the start of each spray run, the substrates were preheated to above 300 °C by the plasma before initiating delivery of the liquid feedstock.

2.2. Electrolyte characterization

2.2.1. Deposition efficiency

Electrolyte deposition efficiencies (DEs) were calculated as the coating weight divided by the weight of YSZ feedstock that was fed when the torch was directly in front of the substrate (i.e. when the central axis of the torch intersects the substrate). For the SPPS coatings, an equivalent feedstock weight was calculated by assuming that the precursors fully reacted with oxygen to form the target coating material.

2.2.2. Microstructure evaluation

Coating cross-sections were imaged using a scanning electron microscope (SEM) (JSM6610, JEOL Ltd, Tokyo, Japan) operating in backscattered electron mode with an accelerating voltage of 15 kV. Samples were mounted in epoxy, sectioned using a diamond saw, remounted in epoxy, polished using standard metallographic methods, and then carbon coated. Average coating thicknesses were determined at 150× magnification by image analysis of 4 unique micrographs of each electrolyte on the bi-layer anode substrates or 2 micrographs of each electrolyte on the porous steel substrates.

2.2.3. Permeability testing

Air leak rates were measured across 0.87 cm^2 electrolyte areas under pressure differentials of up to 4.1 kPa. Corresponding permeability values were calculated by Darcy's law. The measured pressure differential was corrected to subtract the substrate component after separate leak testing was performed on the substrates to determine their pressure differential versus leak rate behaviour. More details on the permeability testing procedure are provided elsewhere [20].

2.3. Electrochemical testing

Electrochemical testing was performed on cells having electrolytes deposited on the bi-layer anode substrates. To form complete cells, $La_{0.6}Sr_{0.4}Co_{0.2}Fe_{0.8}O_{3-\delta}$/$Ce_{0.8}Sm_{0.2}O_{2-\delta}$ (LSCF/SDC) composite cathodes were deposited on the electrolytes by dry powder plasma spraying, as described elsewhere [21]. The cells had active areas of 1 cm^2.

Table 2
Plasma conditions for electrolyte deposition.

Identifier	102 kW	112 kW	160 kW
Torch power (kW)	102 ± 1	112 ± 1	160 ± 1
Nozzle diameter (mm)	7.9 (5/16″)	9.5 (3/8″)	9.5 (3/8″)
Plasma gas flow rate (slpm)	275	275	275
Ar (%)	60	55	25
N_2 (%)	35	40	70
H_2 (%)	5	5	5
Current (A)	525	600	750
Stand-off distances (mm)	65 & 75	85 & 100	90 & 130

Table 3
Substrate composition and properties (±values indicate standard deviation).

Substrate identifier	Porous steel	Bi-layer anode
Support (430 stainless steel)	MG 0.2 μm	MG 1 μm
Electrode bridging layer	None	Dry powder plasma sprayed Ni–YSZ
Electrode functional layer	None	Suspension plasma sprayed Ni–YSZ
Average electrode thickness (μm)	N/A	64 ± 11
Average roughness – R_a (μm)	2.3 ± 0.7	5.4 ± 1.3
Average permeation rate (sccm kPa^{-1} cm^{-2})	1.02 ± 0.10	1.40 ± 0.15

The cell test station was developed in-house, and a schematic of the sample holder is given in Ref. [19]. The anode and cathode gas chambers were isolated using a compressible vermiculite-based gasket (Flexitallic L.P., Deer Park, TX). Voltage/current behaviour was characterized using a Solartron 1470E multi-channel potentiostat combined with a 1260 frequency response analyzer (London Scientific, London, ON, Canada). Cell testing was performed with a furnace temperature of 750 °C. OCV and polarization data were obtained with an anode gas flow rate of 400 sccm of H_2, humidified with approximately 3 vol.% H_2O, and a cathode gas flow rate of 1000 sccm of air. These gas flow rates were used to ensure sufficient fuel and oxidant supply to the active regions of the electrodes. H_2 diffusion was particularly limited by the metal supports, which were not originally developed for SOFCs. Our research group is currently developing metal supports in-house to better enable H_2 diffusion to the anode, and in future studies, the effect of lower gas flow rates on cell performance will be investigated.

2.3.1. Series resistance determination

Due to gas leakage through the electrolyte, combustion raises the internal cell temperature above the furnace temperature. The temperature increase varies from cell to cell, depending on the permeability of the electrolyte and the gas transport characteristics of the electrodes and metal support. For comparing electrolytes, it was preferred to have R_s values at a consistent temperature because ionic conductivity is strongly temperature-dependent. Therefore, a procedure was developed to correct the R_s values to 750 °C, which involved repeat measurements of R_s with various anode gas dilutions.

The temperature correction procedure relied upon four assumptions. First, for a given cell, it was assumed that the amount of combustion and the increase in electrolyte temperature above 750 °C was linearly proportional to the H_2 concentration of the anode gas (ϕ_{H_2}). Second, it was assumed that the conductivity versus temperature behaviour of the plasma sprayed electrolyte was the same as that of bulk YSZ. Plasma sprayed YSZ coatings have previously displayed Arrhenius-type conduction behaviour with activation energies close to that of bulk YSZ [22]. Third, it was assumed that the electrolyte temperature was uniform throughout the active region of the cell. Finally, it was assumed that R_s was entirely due to the ionic resistance of the electrolyte. The step-by-step R_s temperature correction procedure is described below.

1. For each cell, impedance tests were performed at OCV with anode gas mixtures of 100, 70, and 40 vol.% H_2, balance N_2, humidified with approximately 3 vol.% H_2O. From the impedance data, R_s values were determined by equivalent circuit fitting using ZView software (Scribner Associates Inc., Southern Pines, NC). This fitting was performed to correct the impedance data for inductance. The equivalent circuit was similar to that used by Barfod et al. [23], and consisted of a resistor for R_s, an inductor, and 4 parallel resistor-constant phase element pairs.
2. The curve in Fig. 2 plots the ratio of conductivity at a given temperature to conductivity at 750 °C ($\sigma_T/\sigma_{750°C}$) for bulk YSZ. As $1/R_s$ is linearly proportional to conductivity, it was assumed that the $(R_s)_{750°C}/(R_s)_T$ values for the cells would match the $\sigma_T/\sigma_{750°C}$ trend for bulk YSZ.
3. For a given anode gas H_2 concentration, the electrolyte temperature was estimated as:

$$T_{\text{electrolyte}} = 750°\text{C} + A \times \phi_{H_2}$$

Where A is a proportionality constant that is set by minimizing the difference between the $(R_s)_{750°C}/(R_s)_T$ values and the $\sigma_T/\sigma_{750°C}$ values for bulk YSZ (see Fig. 2).

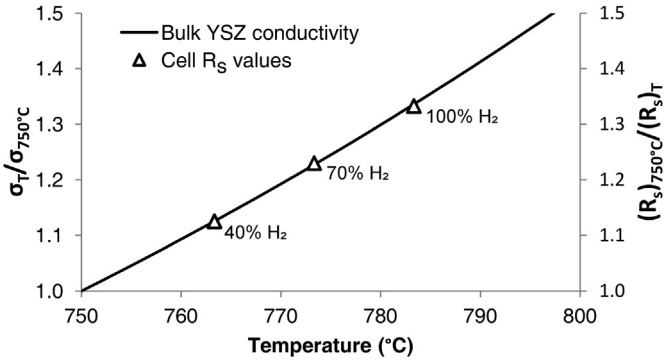

Fig. 2. $(R_s)_{750°C}/(R_s)_T$ values from a sample cell after determining the best value for A. Bulk YSZ $\sigma_T/\sigma_{750°C}$ curve determined from data in Ref. [26].

4. R_s at 750 °C was then estimated by extrapolating along the $\sigma_T/\sigma_{750°C}$ curve for bulk YSZ.

3. Results and discussion

3.1. Deposition efficiency

Fig. 3 shows average electrolyte DEs with the porous steel substrates. Each column represents an average of 2 samples deposited during the same spray run. Maximum sample-to-sample variance was 3% and more typically less than 1%. It was not determined what fraction of this range was due to process variance and what fraction was due to slight differences in sample masking (i.e. small changes in the area of the sample exposed to the plasma due to material accumulation around the mask edges). Nonetheless, sample-to-sample DE variation was small. With the bi-layer anode substrates, the Ni partially oxidizes during electrolyte deposition, so accurate DE measurements could not be obtained without performing an additional reduction step prior to sample weighing. However, estimates for electrolyte DE on the bi-layer anode substrates suggest that they were very similar to those on the porous steel substrates.

Reductions in DE occur for multiple reasons. YSZ may evaporate in the plasma, or it may resolidify prior to impact and bounce off of the substrate surface instead of adhering. YSZ particles smaller than 1 μm have very low velocity normal to the substrate at impact because they are easily deflected by the curving plasma plume [8]. The smallest particles may not adhere to the substrate or they may not impact at all if they are too thoroughly entrained within the plasma gas. With the 102 and 112 kW plasmas, higher DEs were obtained with suspension 2 than with suspension 1. These

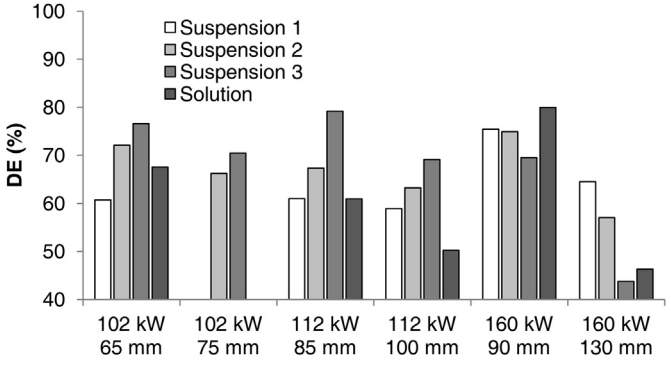

Fig. 3. Electrolyte DEs on porous steel substrates.

suspensions were made with the same powder but suspension 1 was entirely water-based and suspension 2 was made with the water/ethanol/ethylene glycol mixture. This result suggests that combustion did increase the degree of particle melting at impact. With the 160 kW plasma, suspension 2 provided no advantage, likely because the plasma enthalpy alone was sufficient for thorough particle melting.

Suspensions 2 and 3 were made from the same liquid but differently sized powders (d_{50} = 2.6 μm and d_{50} = 0.6 μm, respectively). Higher DEs were obtained with the smaller powder with the 102 and 112 kW plasmas but not the 160 kW plasma. The smaller particles likely melted more readily with the lower energy plasmas but also volatilized more readily with the 160 kW plasma. With all plasma conditions, the decrease in DE with increasing stand-off distance was more significant with the smaller particles. This behaviour was likely due to more resolidification of the smaller particles as the plasma cooled.

DE trends with the solution feedstock are more challenging to interpret than those of the suspension feedstocks. At the shorter stand-off distance tested with each plasma condition, solution DEs were comparable to those of the suspensions. As the stand-off distances were increased, solution DEs dropped substantially, which suggests that resolidification was occurring.

3.2. Permeability and microstructure

Electrolyte permeability values are plotted in Fig. 4. In Fig. 4a, no values are plotted for suspension 3 with the 160 kW plasma at 130 mm. This was the thinnest electrolyte at 24 μm thick, and previous trials with the porous steel substrates found that an electrolyte thickness of approximately 25 μm was required to bridge the surface pores so that permeability values would be comparable to those at the target thickness of 35 μm. With all deposition conditions, electrolyte permeabilities were higher on the bi-layer anode substrates than they were on the porous steel substrates. Segmentation cracks were found to varying degrees in all electrolytes on the bi-layer anode substrates, but these cracks were not observed in any electrolytes on the porous steel substrates. The reduction of segmentation cracking in electrolytes deposited directly on metal supports has previously been attributed to the removal of the thermally-insulating electrode layer between the electrolyte and the metal support [10]. In the SPPS coatings, segmentation cracking appeared to be no more severe than it was in the comparable SPS coatings, which suggests that the solution was fully treated in the plasma before impact. Previous studies have shown that segmentation cracks can form in SPPS coatings when untreated precursor deposits on the substrate and is subsequently pyrolysed by high surface temperatures or heat from the plasma [24].

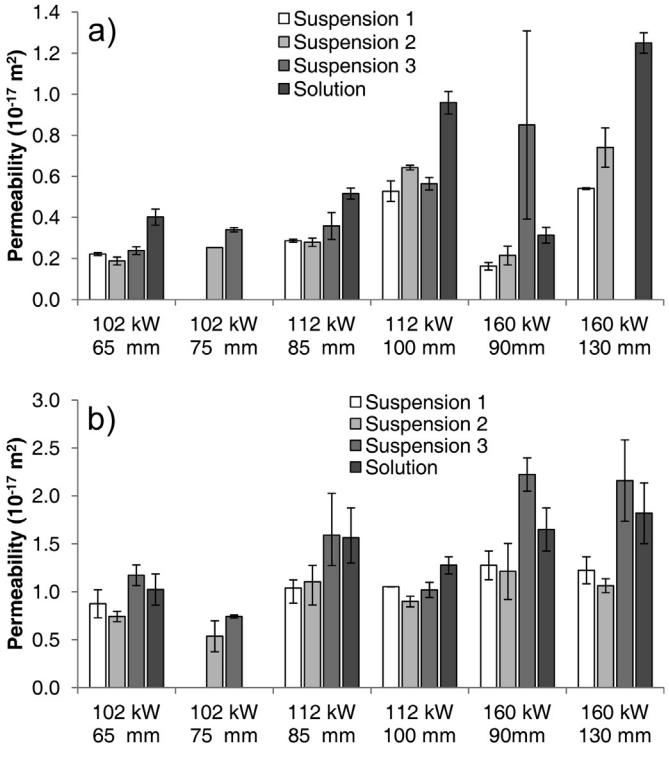

Fig. 4. Average electrolyte permeability: a) on porous steel substrates; b) on bi-layer anode substrates. (Error bars show range of two samples.)

On both types of substrate, permeabilities were generally lower for electrolytes made from suspensions 1 and 2 (d_{50} = 2.6 μm) compared to the other feedstocks. In cross-section images, these electrolytes (Fig. 5a–d) had lower surface roughness and fewer and less severe regions of concentrated porosity compared to the electrolytes made from suspension 3 (d_{50} = 0.6 μm) (Fig. 5e) and the solution (Fig. 5f). Regions of concentrated porosity are likely formed by small droplets with low momentum impacting the substrate at shallow angles [8,25].

On the porous steel substrates, the electrolyte with the lowest permeability was produced from suspension 1 with the 160 kW plasma at 90 mm. The high energy plasma provides for complete feedstock treatment, and the short stand-off distance and relatively large particles minimize resolidification prior to impact. However, on the bi-layer anode substrates (Fig. 5a and b), this electrolyte contains a large number of segmentation cracks due to the large temperature gradient between the electrolyte and metal support during deposition. The electrolyte with the lowest permeability on the bi-layer anode substrates was produced from suspension 2 with the 102 kW plasma at 75 mm. This electrolyte is relatively free of segmentation cracks and concentrated porosity, and provides even coverage of the underlying substrate features (Fig. 5c and d). However, the average air leak rate of this electrolyte is approximately 5× higher than that of the vacuum plasma sprayed electrolytes from the German Aerospace Center (DLR) [2].

3.3. Electrochemical performance

Sample polarization curves at 750 °C are presented in Fig. 6 from cells with bi-layer anode substrates and LSCF/SDC cathodes. While the electrodes were nominally the same in all cells, polarization resistance (R_p) varied between cells so the variation between curves in Fig. 6 was not entirely due to electrolyte performance. Accordingly, the OCV and R_s data are more specific performance indicators for electrolytes, which are the focus of this article. Of the curves shown in Fig. 6, the suspension 2: 102 kW @ 75 mm cell had the highest OCV (1.000 V) of all cells tested and the suspension 3: 102 kW @ 65 mm cell had the highest peak power density (599 mW cm^{-2}). The solution: 160 kW @ 90 mm cell in Fig. 6 was the highest performing cell tested with an SPPS electrolyte.

Cell R_s is typically dominated by electrolyte ionic resistance ($R_{s,electrolyte}$), but also includes contact resistance ($R_{s,contact}$). The standard procedure for estimating $R_{s,contact}$ involves testing multiple cells with electrolytes made using identical deposition conditions but having different thicknesses. From a plot of R_s against electrolyte thickness, $R_{s,contact}$ can be estimated by fitting a linear curve through the data and extrapolating to a thickness of zero. Initial attempts were made to estimate $R_{s,contact}$ using this procedure, though widely varying estimates for $R_{s,contact}$ were obtained with different electrolyte deposition conditions. Unfortunately,

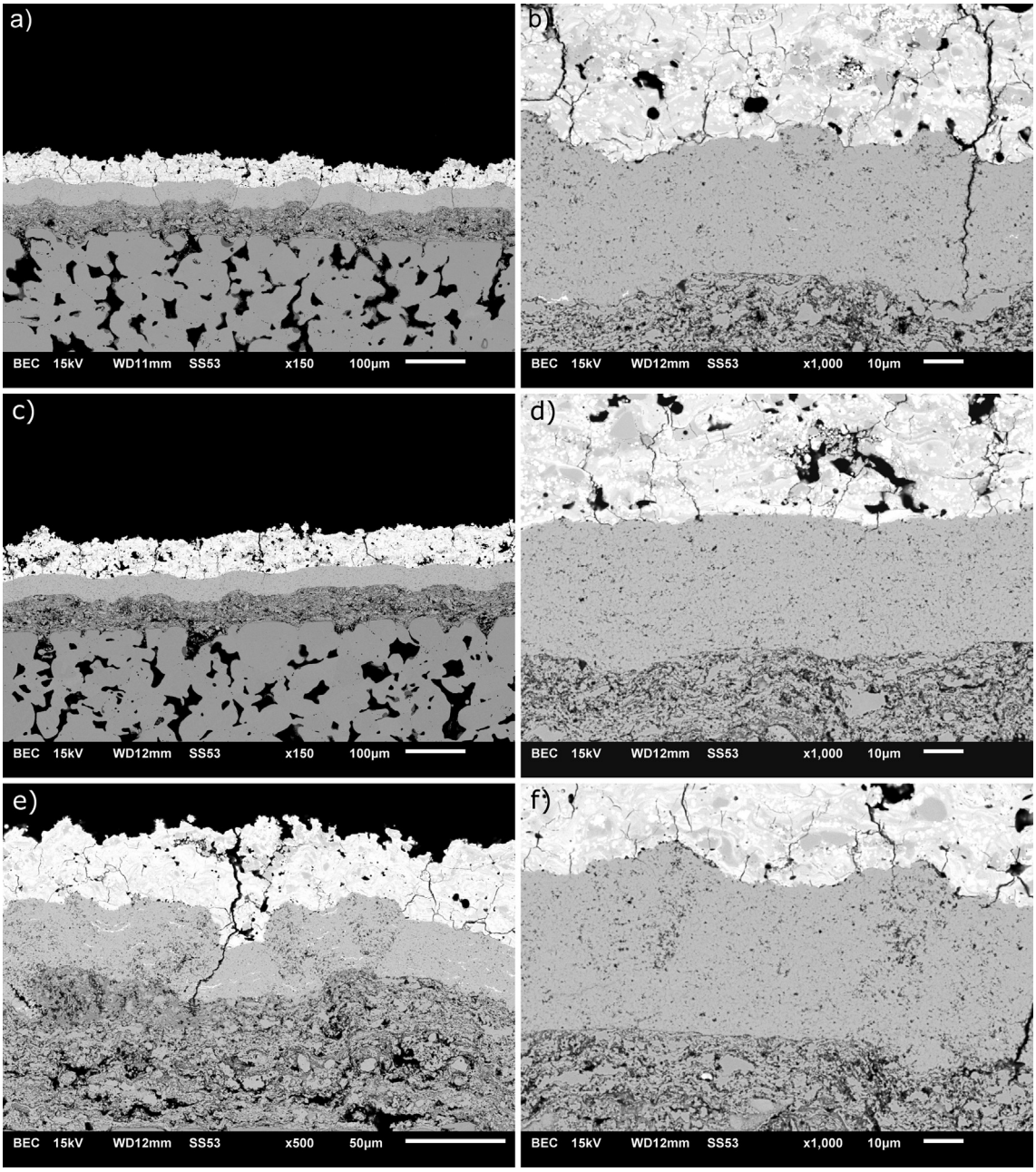

Fig. 5. Sample cross-section images of electrolytes on bi-layer anode substrates with cathodes deposited on electrolytes: a), b) suspension 1: 160 kW @ 90 mm; c), d) suspension 2: 102 kW @ 75 mm; e) suspension 3: 160 kW @ 90 mm; f) solution: 160 kW @ 90 mm.

with thin SPS or SPPS electrolytes, the assumption of a linear relationship between R_s and thickness does not apply because electrolyte microstructures vary with thickness. Near the anode interface, local electrolyte porosity can be higher than bulk porosity as it bridges uneven anode surface features. As thickness increases, undesirable features like concentrated porosity and segmentation cracks become more severe, though the change in severity with thickness depends on the deposition conditions and liquid feedstock used.

Fig. 7 plots electrolyte thickness (t_e) divided by R_s, with no value for $R_{s,contact}$ subtracted from R_s for the reasons discussed in the previous paragraph. t_e/R_s is analogous to conductivity. For a fair comparison between the various electrolytes, thicknesses were between 30 and 40 µm for all samples except where indicated on the figure. In a previous study on cells with SPS electrolytes, $R_{s,contact}$ was estimated to be in the range of 6–27% of R_s at 750 °C [5]. Therefore, actual electrolyte conductivities would be slightly higher than the t_e/R_s values in Fig. 7. The conductivity of bulk YSZ at 750 °C is approximately 3.3×10^{-2} S cm^{-1} [26], and for the most conductive electrolyte in Fig. 7, t_e/R_s is 35% of this value. Due to limited test station access, it was not possible to test multiple samples for all deposition condition/feedstock combinations. Repeat tests were prioritized for samples with the highest promise for overall performance (low R_s and high OCV).

In general, the conductivities of electrolytes made with the 102 kW plasma at 65 mm and the 160 kW plasma at 90 mm were comparable. The 102 kW plasma was produced with a smaller torch nozzle, highlighting the importance of plasma velocity for

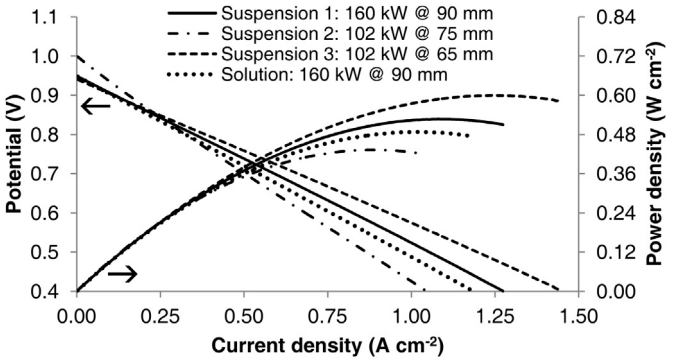

Fig. 6. Sample cell polarization curves at 750 °C. Anode gas was H_2 humidified with approximately 3 vol.% H_2O and cathode gas was air. (Polarization data were not corrected for combustion-related temperature deviation from 750 °C.)

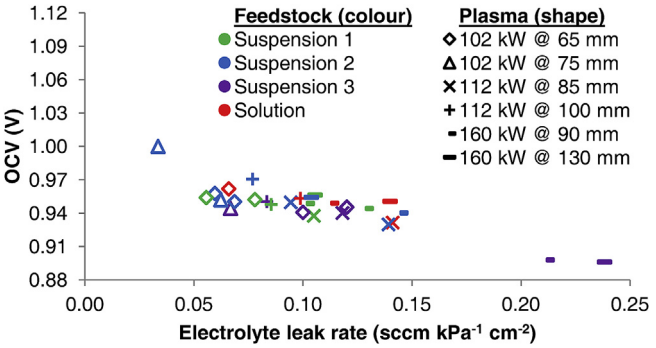

Fig. 8. Cell OCVs in 750 °C furnace versus electrolyte leak rate. Anode gas was H_2 humidified with approximately 3 vol.% H_2O and cathode gas was air.

producing conductive electrolytes. With the 102 and 112 kW plasmas, electrolytes made from suspension 3 had the highest conductivity, possibly because its smaller (d_{50} = 0.6 μm) particles melted more readily compared to the larger (d_{50} = 2.6 μm) particles in suspensions 1 and 2. The addition of ethanol and ethylene glycol to the suspension improved conductivity with the 102 kW plasma but did not provide any substantial advantage with the 112 and 160 kW plasmas. The conductivities of the SPPS electrolytes were generally comparable to those of the SPS electrolytes.

Fig. 8 plots cell OCVs against the electrolyte leak rates that were measured during permeability testing. OCV generally increased with decreasing leak rate, as has been previously reported [2,5], so the permeability data in Fig. 4b are useful for anticipating electrochemical performance. However, there is scatter in Fig. 8 because OCV depends on the gas compositions in the electrodes, and gas transport in the electrodes and metal supports was not perfectly uniform from cell to cell. For the furnace temperature and gas supply used for these tests, the Nernst equation gives a theoretical OCV of 1.11 V, which is 0.11–0.21 V above the measured values.

3.4. Selection of feedstock and deposition conditions

The selection of the most suitable feedstock and plasma conditions depends on multiple considerations. For the SOFC electrolyte, the key performance metrics are OCV and R_s. Unfortunately, maximizing OCV and minimizing R_s can be competing objectives. Dense coatings with good conductivity often contain more segmentation cracks and concentrated porosity, which harm OCV.

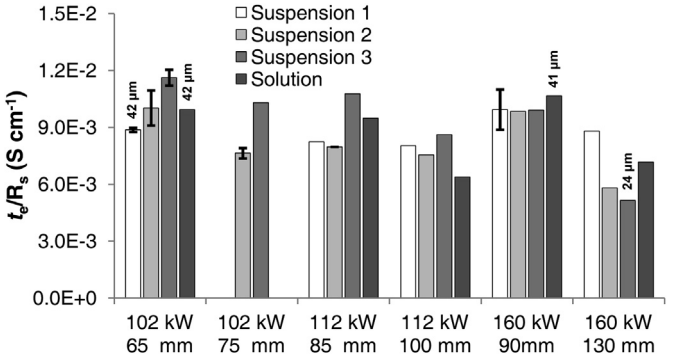

Fig. 7. Electrolyte thickness divided by R_s at 750 °C. (R_s was corrected for temperature as described in Section 2.3.1. All electrolytes were between 30 and 40 μm thick unless indicated on figure. Error bars indicate range if two samples were tested. If no error bars are shown, only one sample was tested.)

Further complicating matters is that the electrolyte microstructure is strongly dependent on the characteristics of the substrate. Thinner, more thermally conductive electrode layers permit the use of higher power spray conditions to produce denser electrolytes without forming segmentation cracks. Smoother anodes enable the use of deposition conditions and feedstocks that would form severe regions of concentrated porosity on rougher substrates. Finally, process DE cannot be neglected for its effect on material costs.

Gas leakage across the electrolyte reduces power output, wastes fuel, and increases cell degradation, so improving OCV is a high priority. Electrolytes made from the solution and suspension 3 (particle d_{50} = 0.6 μm) had higher permeabilities than those made from suspensions 1 and 2 (particle d_{50} = 2.6 μm). Accordingly, the larger feedstock powder used for these suspensions is considered preferable, despite the higher conductivity electrolytes that were produced with suspension 3 and the solution. Going forward, two deposition condition/feedstock combinations show particular promise for achieving high OCVs without overly sacrificing conductivity. First, the electrolytes made from suspension 2 with the 102 kW plasma and a 75 mm stand-off distance had the lowest permeability on the bi-layer anode substrates and achieved the highest OCV. This coating was relatively free of segmentation cracks and concentrated porosity but also had a t_e/R_s value of 7.6×10^{-3} S cm^{-1} and a DE of 66%. Therefore, this electrolyte is well suited for deposition on rough and/or thick electrode layers. However, if the anode can be made thinner and smoother, suspension 1 with the 160 kW plasma and a 90 mm stand-off should produce better performing electrolytes. This deposition condition/feedstock combination achieved the lowest permeability on the porous steel substrates, on which segmentation cracking did not occur and concentrated porosity formation was less severe. This electrolyte had a t_e/R_s value of 9.9×10^{-3} S cm^{-1} and a DE of 75%. Our research group has recently developed cells with considerably thinner and smoother anodes than the bi-layer anodes used in this study, and cell performance data with these anodes will be reported in a subsequent publication.

State-of-the-art metal-supported SOFCs produced by the Risø National Laboratory for Sustainable Energy contain 12 μm thick electrolytes produced by sintering [1]. With plasma spraying, it may not be possible to produce such thin and conductive electrolytes, but plasma spraying should offer production and capital cost advantages over sintering. The German Aerospace Centre (DLR) produces metal-supported SOFCs with 35 μm thick vacuum plasma sprayed-electrolytes, and estimates that 300 100 cm^2 cells h^{-1} can be produced in one spray booth [2]. The DLR cells achieved the Nernst potential and the electrolytes were 5× more gas-tight than the most gas-tight SPS electrolytes produced in this study. However, DLR used dry powder as feedstock, and it should theoretically be possible to obtain comparable gas-tightness with thinner SPS

electrolytes due to the smaller feedstock powders in suspensions and their correspondingly smaller deposits. Reductions in anode thickness and roughness should help improve electrolyte gas-tightness. With further development, it is conceivable that SPS electrolytes that are less than 20 μm thick could achieve comparable gas-tightness to the thicker vacuum plasma sprayed electrolytes. Furthermore, atmospheric SPS offers additional cost advantages because it does not require a vacuum.

Figs. 6–8 present the first electrochemical test data on YSZ electrolytes produced by atmospheric SPPS. These results are preliminary, and with further process improvements, SPPS electrolytes could potentially perform as well as or better than those made by SPS.

4. Conclusions

YSZ electrolytes were deposited by liquid-feed plasma spraying using 3 different suspensions and 1 precursor solution. The various suspensions were used to investigate the importance of powder size distribution and liquid composition. A powder with a d_{50} of 2.6 μm was found to be better than a powder with a d_{50} of 0.6 μm for producing gas-tight electrolytes, as the larger powder resulted in coatings with less concentrated porosity. With lower energy plasmas, the use of a flammable suspension dispersion medium gave higher DEs and conductivities compared to an entirely water-based suspension. With higher energy plasmas, the choice of suspension dispersion medium was less important. The peak DE and conductivity of the electrolytes made from the solution were comparable to the peak values obtained with the suspension electrolytes. However, leak rates through the solution electrolytes were higher than those through the electrolytes made from the suspensions of the larger powders.

The optimal spray condition/feedstock combination depends on the substrate characteristics. A peak OCV of 1.00 V was obtained at 750 °C, though that electrolyte had a t_e/R_s of 7.6×10^{-3} S cm^{-1}. This value is 34% lower than the peak t_e/R_s values, which were measured in cells with denser but less gas-tight electrolytes. If the electrode on which the electrolyte is deposited can be made thinner and smoother, it may be possible to deposit an electrolyte with a t_e/R_s of 9.9×10^{-3} S cm^{-1} and still achieve high OCVs.

Acknowledgements

The authors are grateful for their use of the Centre for Advanced Coating Technologies (CACT) facilities at the University of Toronto, and would like to thank Tiegang Li for his assistance with plasma spraying. The gasket material used for electrochemical testing was provided by Flexitallic L.P. Research and salary funding was provided by the Natural Sciences and Engineering Research Council of Canada (NSERC) and equipment funding was provided by the Canada Foundation for Innovation (CFI) and the Ontario Ministry for Research and Innovation.

References

[1] P. Blennow, J. Hjelm, T. Klemensø, S. Ramousse, A. Kromp, A. Leonide, A. Weber, J. Power Sources 196 (2011) 7117–7125.
[2] P. Szabo, J. Arnold, T. Franco, M. Gindrat, A. Refke, A. Zagst, A. Ansar, ECS Trans. 25 (2009) 175–185.
[3] R. Vaßen, D. Hathiramani, J. Mertens, V.A.C. Haanappel, I. Vinke, Surf. Coat. Technol. 202 (2007) 499–508.
[4] Y. Wang, J.-G. Legoux, R. Neagu, S. Hui, B. Marple, J. Therm. Spray Technol. 21 (2012) 7–15.
[5] D. Waldbillig, O. Kesler, J. Power Sources 196 (2011) 5423–5431.
[6] L. Pawlowski, Surf. Coat. Technol. 203 (2009) 2807–2829.
[7] H.-B. Xiong, J.-Z. Lin, J. Therm. Spray Technol. 18 (2009) 887–895.
[8] J. Oberste Berghaus, S. Bouaricha, J.-G. Legoux, C. Moreau, in: E. Lugscheider (Ed.), Proceedings of the 2005 International Thermal Spray Conference, Basel, Switzerland, pp. 512–518.
[9] D. Soysal, A. Ansar, Surf. Coat. Technol. 220 (2013) 187–190.
[10] M. Marr, O. Kesler, Surf. Coat. Technol. 216 (2013) 289–296.
[11] R. Rampon, O. Marchand, C. Filiatre, G. Bertrand, Surf. Coat. Technol. 202 (2008) 4337–4342.
[12] L. Jia, F. Gitzhofer, J. Therm. Spray Technol. 19 (2010) 566–574.
[13] K. VanEvery, M. Krane, R. Trice, W. Porter, H. Wang, M. Besser, D. Sordelet, J. Ilavsky, J. Almer, Int. J. Appl. Ceram. Technol. 8 (2011) 1382–1392.
[14] J. Irvine, J. Dobson, T. Politova, S. Garca Martn, A. Shenouda, Faraday Discuss. 134 (2007) 41–49.
[15] T. Zhang, Z. Du, S. Li, L. Kong, X. Song, J. Lu, J. Ma, Solid State Ionics 180 (2009) 1311–1317.
[16] C. Muoto, E. Jordan, M. Gell, M. Aindow, J. Therm. Spray Technol. 20 (2011) 802–816.
[17] D. Chen, E. Jordan, M. Gell, Surf. Coat. Technol. 202 (2008) 2132–2138.
[18] C. Metcalfe, J. Kuhn, O. Kesler, J. Power Sources, (2013), http://dx.doi.org/10.1016/j.jpowsour.2013.05.174.
[19] C. Metcalfe, J. Harris, J. Kuhn, M. Marr, O. Kesler, J. Therm. Spray Technol. 22 (2013) 599–608.
[20] M. Marr, O. Kesler, J. Therm. Spray Technol. 21 (2012) 1334–1346.
[21] J. Harris, C. Metcalfe, M. Marr, J. Kuhn, O. Kesler, J. Power Sources 239 (2013) 234–243.
[22] C. Zhang, C.-J. Li, G. Zhang, X.-J. Ning, C.-X. Li, H. Liao, C. Coddet, Mater. Sci. Eng. B 137 (2007) 24–30.
[23] R. Barfod, M. Mogensen, T. Klemensø, A. Hagen, Y.-L. Liu, P. Vang Hendriksen, J. Electrochem. Soc. 154 (2007) B371–B378.
[24] L. Xie, D. Chen, E. Jordan, A. Ozturk, F. Wu, X. Ma, B. Cetegen, M. Gell, Surf. Coat. Technol. 201 (2006) 1058–1064.
[25] K. VanEvery, M. Krane, R. Trice, H. Wang, W. Porter, M. Besser, D. Sordelet, J. Ilavsky, J. Almer, J. Therm. Spray Technol. 20 (2011) 817–828.
[26] J. Fergus, J. Power Sources 162 (2006) 30–40.